Accepted Manuscript

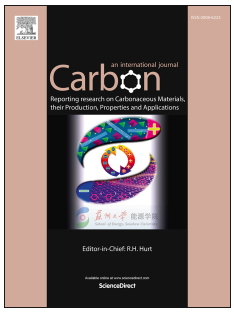

Revealing lattice disorder, oxygen incorporation and pore formation in laser induced two-photon oxidized graphene

Martin E. Mendoza, Erlon H.M. Ferreira, Alexei Kuznetsov, Carlos A. Achete, Jukka Aumanen, Pasi Myllyperkiö, Andreas Johansson, Mika Pettersson, Braulio S. Archanjo

PII: S0008-6223(18)31103-5

DOI: https://doi.org/10.1016/j.carbon.2018.11.070

Reference: CARBON 13687

To appear in: *Carbon*

Received Date: 26 September 2018

Revised Date: 12 November 2018

Accepted Date: 23 November 2018

Please cite this article as: M.E. Mendoza, E.H.M. Ferreira, A. Kuznetsov, C.A. Achete, J. Aumanen, P. Myllyperkiö, A. Johansson, M. Pettersson, B.S. Archanjo, Revealing lattice disorder, oxygen incorporation and pore formation in laser induced two-photon oxidized graphene, *Carbon* (2018), doi: https://doi.org/10.1016/j.carbon.2018.11.070.

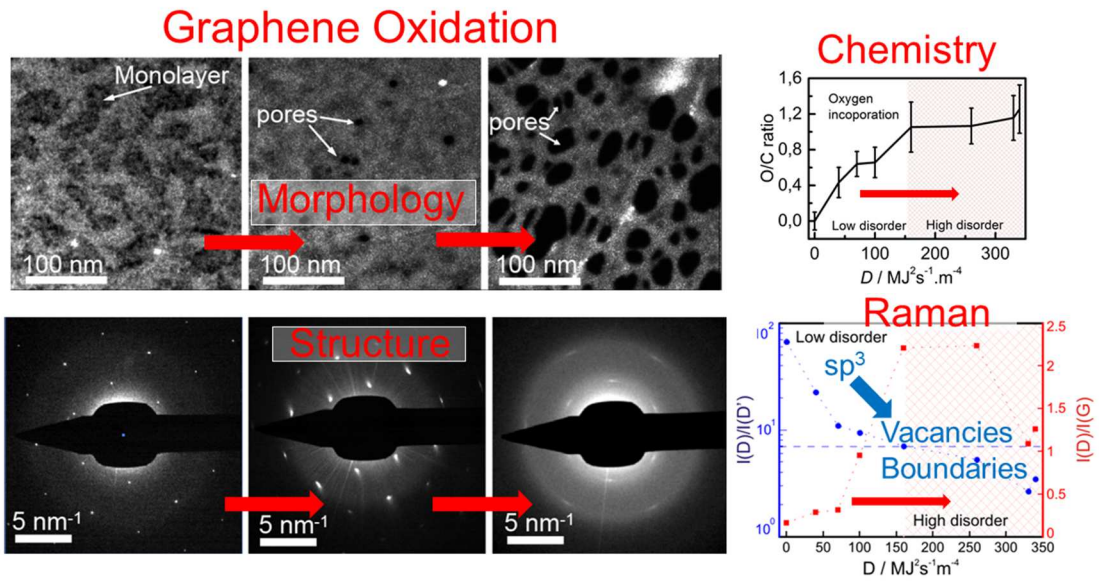

Revealing lattice disorder, oxygen incorporation and pore formation in laser induced two-photon oxidized graphene

Martin E Mendoza[1,2], Erlon H. M. Ferreira[1], Alexei Kuznetsov[1], Carlos A. Achete[1], Jukka Aumanen[3], Pasi Myllyperkiö[3], Andreas Johansson[3, 4], Mika Pettersson[3] and Braulio S. Archanjo[11]

1. Divisão de Metrologia de Materiais, Instituto Nacional de Metrologia, Qualidade e Tecnologia, Duque de Caxias, RJ 25250-020, Brazil

2. Universidad Pedagógica y Tecnológica de Colombia. Avenida Central del Norte 39-115- P.O. Box 150001, Boyacá, Colombia.

3. Department of Chemistry, Nanoscience Center, University of Jyväskylä, P.O. Box 35, Jyväskylä FI-40014, Finland

4. Department of Physics, Nanoscience Center, University of Jyväskylä, P.O. Box 35, Jyväskylä FI-40014, Finland

Abstract

Laser induced two-photon oxidation has proven to be a reliable method to pattern and control the level of oxidation of single layer graphene, which in turn allows the development of graphene-based electronic and optoelectronic devices with an all-optical method. Here we provide a full structural and chemical description of modifications of air-suspended graphene during the oxidation process. By using different laser irradiation doses, we were able to show via transmission electron microscopy, electron energy loss spectroscopy, electron diffraction and Raman spectroscopy how graphene develops from its pristine form up to a completely oxidized, porous and amorphous carbon layer. Furthermore, the gradual control of the oxidation process is used to correlate lattice disorder, oxygen incorporation and pores formation in graphene oxide. This study provides a model system that will benefit research on graphene and other two-dimensional materials.

Keywords

Graphene oxide, Photo-oxidation, TEM, EELS, Raman spectroscopy, Electron diffraction

[1] Corresponding author. E-mail: bsarchanjo@inmetro.gov.br (Braulio S. Archanjo)

1. Introduction

2D materials hold the potential for development of novel applications in electronics, optoelectronics, energy production and storage, sensing and electrochemistry [1-4]. As the most studied 2D material, graphene is a platform to unravel the science behind low dimensional materials. Therefore, many methods have already been used to modify graphene, including different strategies for tailoring its shape [5-8], defect control [9-11], chemical modification [12-15], besides many others. Recently, an all-optical method, namely, two-photon oxidation of graphene was demonstrated, which proved to have some advantages as compared to other oxidation methods, including direct writing of device features with sub-micrometer resolution, high speed and controlled level of oxidation [16-19]. Previous atomic force microscopy (AFM), Raman and X-ray photoelectron spectroscopy (XPS) studies showed a two-photon oxidation process starting with point-like functionalized sites evolving into oxidized islands and then forming a uniform graphene oxide (GO) material mainly composed of hydroxyl (OH) and epoxide (C–O–C) functional groups with a few per cent of carboxylic (COOH) groups [17, 18].

Here in this work we provide further insight into the structure of the laser induced two-photon oxidized graphene via high resolution transmission electron microscopy (HRTEM), electron diffraction (ED) and dark field (DF) images. These results are then correlated with Raman spectroscopy and chemical characterization (O/C ratio) using electron energy loss spectroscopy (EELS).

The highest amount of oxygen incorporation in graphene during laser irradiation in any chemical form is found to be corresponding to O/C ratio close to one. After a certain irradiation dose, no further O/C ratio increase is observed while the graphene structure undergoes profound modifications, evolving from a low disorder regime to a high disorder regime typified by amorphization, formation of pores and rotation of domains. The obtained results benefit the promising research on GO, providing a reference for oxygen incorporation, pore formation and their respective influence in the GO crystal structure.

2. Methods

Single Layer Graphene on a 2000 Mesh Copper TEM Grid was purchased from Graphene Platform Corp. The graphene was suspended over 7.5 μm × 7.5 μm square openings in the TEM grid.

Photo-oxidation of graphene samples was performed using laser irradiation setup described in the previous studies [18]. Briefly, a femtosecond pulsed laser beam (Pharos-10, 600 kHz, Light Conversion) of 540 nm laser pulses with 30 fs pulse duration, 600 kHz repetition rate and varying pulse energy was used for samples irradiation. Patterning was performed in ambient air by the laser beam of 500 nm diameter (estimated at full width at half the maximum, FWHM, of the peak intensity) with sample displacement steps of 100 nm along *x* axis and *y* axis (at the end of the course along *x* axis), and step scan rates of 0.1 sec/step and 0.2 sec/step. The total illuminated area was about 5 μm × 5 μm. In order to provide an irradiation dose comparative basis for observed irradiation effects induced by different laser intensities and/or scan rates, we defined a dose parameter *D* which relates to the average power as shown in Table S1 of the support information. The details of calculating *D* can be also found in the support information. The irradiation average power was varied from 1 μW to 2.9 μW, where at higher average powers (> 2.9 μW), ablation of graphene took place. Therefore, irradiation of graphene can be divided in three fluence levels: low irradiation dose (laser power and dose parameter *D* below 1.3 μW and 70 $MJ^2/(s.m^4)$ respectively), intermediate irradiation dose (laser power from 1.6 μW to 2.0 μW and 100 $MJ^2/(s.m^4) < D < 160$ $MJ^2/(s.m^4)$) and high irradiation dose (laser power 2.5 μW, twofold 2.0 μW and 2.9 μW, and 260 $MJ^2/(s.m^4) < D < 340$ $MJ^2/(s.m^4)$).

For TEM observations, a probe corrected FEI-Titan 80-300 at 80 kV operation voltage was used. Selected area electron diffraction (ED), having illuminated areas with the diameter of about 180 nm, and high-resolution transmission electron microscopy (HRTEM) image modes were used to visualize the structural changes in the oxidized graphene. Dark field (DF) images were taken at intermediate magnification (50 kx). To determine the diffraction profiles the Digital Micrograph software (version 1.85) was used for images acquisition and processing.

Chemical characterization was performed using electron energy loss spectroscopy (EELS) with monochromator in STEM mode. Zero loss peak (ZLP) resolution measured at full width half maximum was 0.2 eV using convergence angle α = 27.3 mrad, camera length L = 60

mm, GIF entrance aperture = 2.5 mm and dispersions 0.01 eV/ch or 0.2 eV/ch. For C and O measurements, three spectra were collected for better data statistics. For each collection, the electron beam scanned areas of 300 nm × 300 nm in neighbor regions, with a beam current of 0.5 nA and a total collection time of 70 s. The background was fitted using a power law model and subtracted from the spectra. The Hartree-Slater model was used for cross section estimation. The EELS quantifications were performed using Gatan Digital Micrograph software (TM) 3.11.0 for GMS 1.6.0.

For Raman measurements, a Witec Alpha A/R 300 instrument with backscattering geometry, laser of 532 nm and power at the sample of 0.1 mW with a 100x (N.A. 0.90) objective was used. For better statistics, we measured Raman spectra in few locations inside at least two different regions irradiated to the same dose. All Raman spectra were fitted using three Lorentzian curves corresponding to the D, G and D' bands.

3. Results and Discussions

3.1 HRTEM, ED and DF

A set of high resolution transmission electron microscopy images (HRTEM), electron diffraction (ED) and dark field (DF) images taken at different regions for different irradiation doses are presented in Fig. 1. The HRTEM images of the non-irradiated (pristine) graphene (Fig. 1a) show two distinct regions. The brighter region corresponds to a highly ordered crystalline monolayer graphene, which is confirmed by the Fourier filtered image in the inset. The other darker region is a thicker and disordered layer, which we argue is due to polymer contamination from the transfer of graphene onto the TEM grid. These polymer contaminated regions of pristine graphene will be further discussed in section 3.3. Although laser irradiation leads to generation of disorder in graphene, the HRTEM results do not show significant differences between pristine and lightly irradiated (dose parameter $D < 70$ MJ^2/(s.m^4)) graphene. Indeed, by analyzing Fig. S1c and S1e, highly ordered regions can be seen in the graphene layer at low irradiation doses. Even at intermediate irradiation doses (100 MJ^2/(s.m^4) $< D <$ 160 MJ^2/(s.m^4)), highly crystalline regions can still be found, as can be seen for the region irradiated at 160 MJ^2/(s.m^4) at the top right of Fig. 1b. As we go for higher irradiation doses (260 MJ^2/(s.m^4) $< D <$ 340 MJ^2/(s.m^4)), the crystalline regions become rare, and eventually completely absent as

observed in Fig. 1c. For HRTEM images of all irradiated regions used in this work, see Fig. S1 in the support information available online.

Using ED, we can observe the evolution of the graphene structure from pristine (diffraction dots in Fig. 1d), through defective (radial spot broadening in Fig. 1e), until highly disordered (lateral spot broadening becoming diffuse rings in Fig. 1f) demonstrating the increasing structural disorder as irradiation dose increases. In section 3.2 below, the ED patterns are analyzed in details.

The DF images (Figs. 1g, 1h and 1i) also corroborate the evolution of the sample's structure from pristine to highly disordered graphene. In Fig. 1g the darker zones correspond to clean monolayer graphene which appears as brighter areas in HRTEM of Fig. 1a. The brighter zones in DF images are identified as polymer contaminated regions on top of highly crystalline graphene. The scattered electrons coming from polymer contaminated regions are added to the signal from highly crystalline graphene support film, which explains why the disordered regions in HRTEM images are brighter in DF images. Using Fig. 1g, we estimate that the polymer contamination covers about 50% of the suspended graphene surface. Typically, graphene is grown on copper or nickel foil using CVD (chemical vapor deposition), and poly(methyl methacrylate) (PMMA) or other polymers are used to transfer it to TEM grids or to any other substrate [4]. The polymer removal usually leaves thin contamination layers on top of graphene, being the main reason for the poorly ordered regions seen in HRTEM images. Although less common for high quality CVD grown graphene, these disordered regions in HRTEM images can also come from few layered graphene and amorphous carbon that might grow/deposit on copper or nickel foil [4, 20].

At D of 160 $MJ^2/(s.m^4)$, there is almost no contrast between darker (thin highly crystalline graphene) and brighter (disordered/contaminated) regions in DF image of Fig. 1h, although the ED in Fig. 1e shows slightly broadened spots with hexagonal symmetry pattern. Therefore, one can conclude that crystalline graphene (with a certain degree of disorder) is present at this irradiation dose and the small difference in contrast in the DF image (Fig. 1h) is probably due to the evaporation of the contamination layer. This point will be further discussed in section 3.3.

Furthermore, for the doses as low as 100 $MJ^2/(s.m^4)$ (Fig. S2c) pores can be seen. Especially for intermediate dose irradiated graphene, small pores having around 10 nm diameter (black regions highlighted by the arrows in Fig. 1h) are visible everywhere in the graphene layer. The pore size increases up to several tens of nanometers for higher dose irradiated graphene, as shown in Fig. 1i (see also Fig. S2 in the support information).

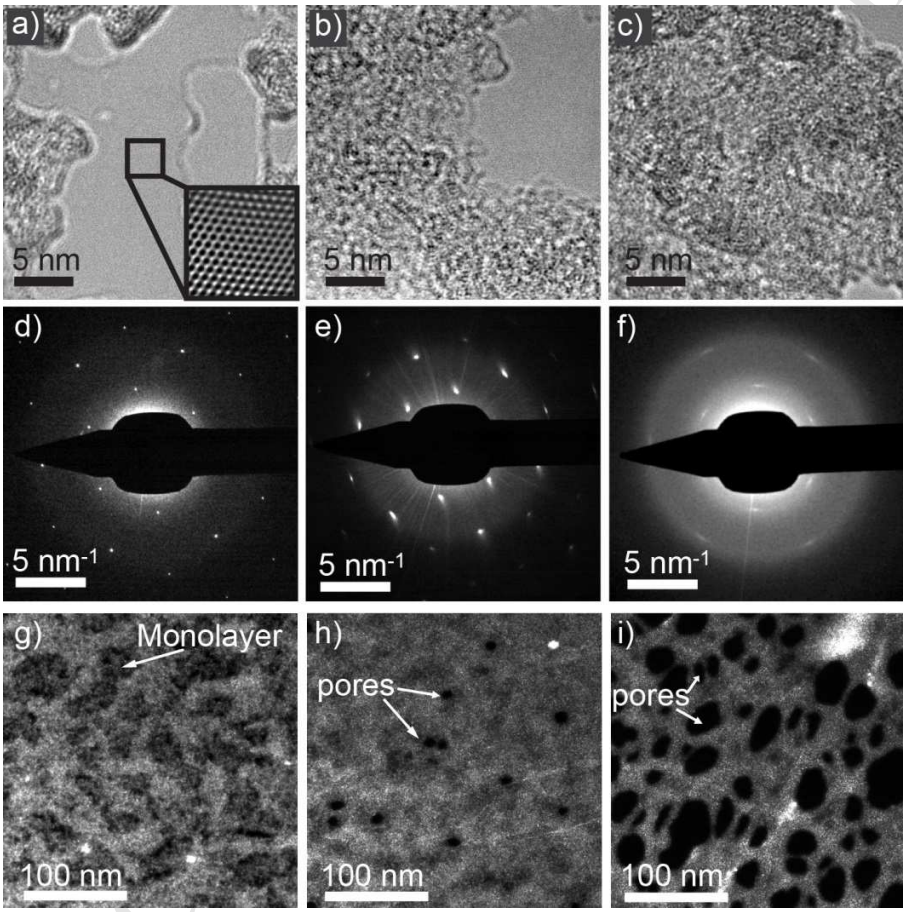

Fig. 1. General structural and morphological behavior of two-photon oxidized graphene with different irradiation doses via transmission electron microscopy (TEM): pristine (a, d and g), intermediated radiation dose *D* of 160 $MJ^2/(s.m^4)$ (b, e and h) and high irradiation dose *D* of 340 $MJ^2/(s.m^4)$ (c, f and i). HRTEM images are shown in panels (a), (b) and (c) where the inset in panel (a) is a Fourier filtered image showing the periodic structure of a monolayer region. Intensity of ED reflections are displayed in panels (d), (e) and (f). In panels (g), (h) and (i) DF

images are shown at intermediate magnification. See Figs. S1 and S2 in the support information available online for complementary information.

3.2 Structural characterization

There is a vast literature where different types of defects and microstructure features of crystalline solids are studied by analyzing X-ray or neutron diffraction-peak profiles [14, 21, 22]. In the last few years, with the raise of nanotechnology and nanoscience, electron diffraction (ED) in a TEM is becoming more and more attractive since it has the ability to probe very small volumes, as required by these fields [23-25]. Analogously to X-ray diffraction, the intensity profile of each individual reflection in ED is affected by defects. This effect can be used to relate the ED peak profile parameters (for example, peak broadening) with microstructural features of a material. The analysis and interpretation of the ED peak profiles can be based, for example, on the statistical approach by a Fourier series [26] that minimizes the need for *a priori* assumptions with respect to the defects characteristics. However, such a method requires considerable effort to separate the sample´s contribution from instrumental contribution to peak profile. In case of ED, the determination of such a contribution is a challenging task prone to considerable experimental inaccuracies. On the other hand, much simpler approaches, as for example the Scherrer model, and simplified assumptions about microstructural details (e.g. about crystallites size distribution) provide mostly estimations of microstructural characteristics. Nevertheless, a simple approach to evaluation of microstructural characteristics can be very useful in case of comparative analysis. Therefore, efforts to correlate the peak width of the ED experiments with the level of structural disorder are of great interest. Indeed, ED and HRTEM have already been used to study graphite [27], graphene [28, 29] and GO [30, 31] in a few cases. Usually the analysis is very local and limited to HRTEM [32, 33] in which a disorder coefficient [27] or an average defect density [29] (in terms of the ED spots broadening) is determined.

Here, for a better understanding of the structural evolution of two-photon irradiated graphene the electron diffraction is further analyzed and the width of the spots in ED is measured in order to associate these changes with the alterations in size of crystallite domains, micro strains, sheet roughness and domain fragmentation. The electron diffraction of graphene irradiated to 260 $MJ^2/(s.m^4)$ is shown in Fig. 2a. The inset of Fig. 2a highlights the diffraction peak broadening in radial direction (along the reciprocal lattice vector), as well as diffraction peak streaking, ϕ, along the tangential direction (perpendicular to the reciprocal lattice vector). The intensity profiles of $(1\bar{1}20)$ reflections measured along the reciprocal lattice vector are plotted in Fig. 2b. Fig. 2c shows the average full width at half maximum (FWHM) of the

intensity profiles of $(\bar{1}010)$, $(\bar{2}110)$ and $(\bar{2}200)$ reflections as the function of the dose parameter *D*. The determination of FWHM was performed by profile fitting of the average of three equivalent peaks using a Lorentz function. The average of FWHMs of peaks profiles are determined by fitting the different reflections in ED pattern. Since single reciprocal spaces are measured in most of ED patterns (it is not the case of graphene illuminated under 40 $MJ^2/(s.m^4)$ as shown in Fig. S1d, where less intense spots from a second grain can be seen), the illuminated areas in these experiments, with a diameter of 180 nm, cover single graphene grains.

For *D* up to 70 $MJ^2/(s.m^4)$ the recorded changes in diffraction patterns are very similar to the one of pristine graphene. The FWHM values of intensity profiles (see Fig. 2c) are nearly equal at respective irradiation doses. Further irradiation results in a rapid increase of FWHM values that reach the magnitudes characteristic of diffuse rings at about 330 $MJ^2/(s.m^4)$. The above results indicate that considerable microstructural changes of pristine graphene start developing after a certain amount of irradiation rather than immediately with initiation of irradiation. One can conjecture that the accumulation of oxygen-containing carbon functional groups is required to onset appreciable structural alterations during irradiation by lasers. This conclusion is supported by EELS measurements presented in next section. Based on FWHM values, the intense transition from lowly disordered to highly disordered graphene (or graphene oxide) occurs between intermediate to high irradiation dose regimes (160 $MJ^2/(s.m^4) < D <$ and 260 $MJ^2/(s.m^4)$). This dose interval correlates well with the nucleation and growth of pores in graphene observed in the TEM studies (see Fig. 1).

The details of microstructural changes of graphene upon irradiation are also reflected in diffraction spots streaking. Generally, one can distinguish two types of streaks: radial streaks (along the Debye-Scherrer rings or perpendicular to the reciprocal lattice vector) and non-radial (linear). The latter type of streaks is related to the kind of relrod features and the former one is related to disorientation of coherently scattering domains. The obtained ED patterns show that the observed streaks are radial. Consequently, one can exclude the occurrence of strongly correlated atomic displacements (atomic linear chains of displacements) that may take place during irradiation, because such defects would produce linear streaks [34]. The formation of the radial streaks also excludes that the buckling of graphene sheet is the only process occurring during irradiation. As shown previously [29], the buckling results in an isotropic broadening of diffraction spots. In the proposed model of buckling, inhomogeneous atomic displacements are

isotropic and produce characteristic micro strain effect in ED pattern which is independent of a direction in the reciprocal space.

In the present study, we estimated the extent of the streaking observed upon the irradiation taking $(11\bar{2}0)$ reflection, for which this effect is more pronouncedly seen. The azimuth angle φ of Debye Scherrer ring covering the observable intensity was approximately 4° at D = 160 $MJ^2/(s.m^4)$ (see inset in Fig. 2a). It increases to approximately 7° at D = 260 $MJ^2/(s.m^4)$ and reaches about 16° at D = 330 $MJ^2/(s.m^4)$. We believe that besides the pore formation, irradiation breaks coherency of graphene domains and the fragments can be disoriented in both in plane and out of plane directions. Oxidation and formation of sp^3 bonds may contribute to fragmentation of graphene crystal and to disorientation of fragments. One cannot exclude the buckling of graphene analogous to the study of Ref. [29]. Most probably both fragmentation and buckling processes are induced by laser irradiation and contribute to the increase of FWHM of radial profiles of diffraction spots.

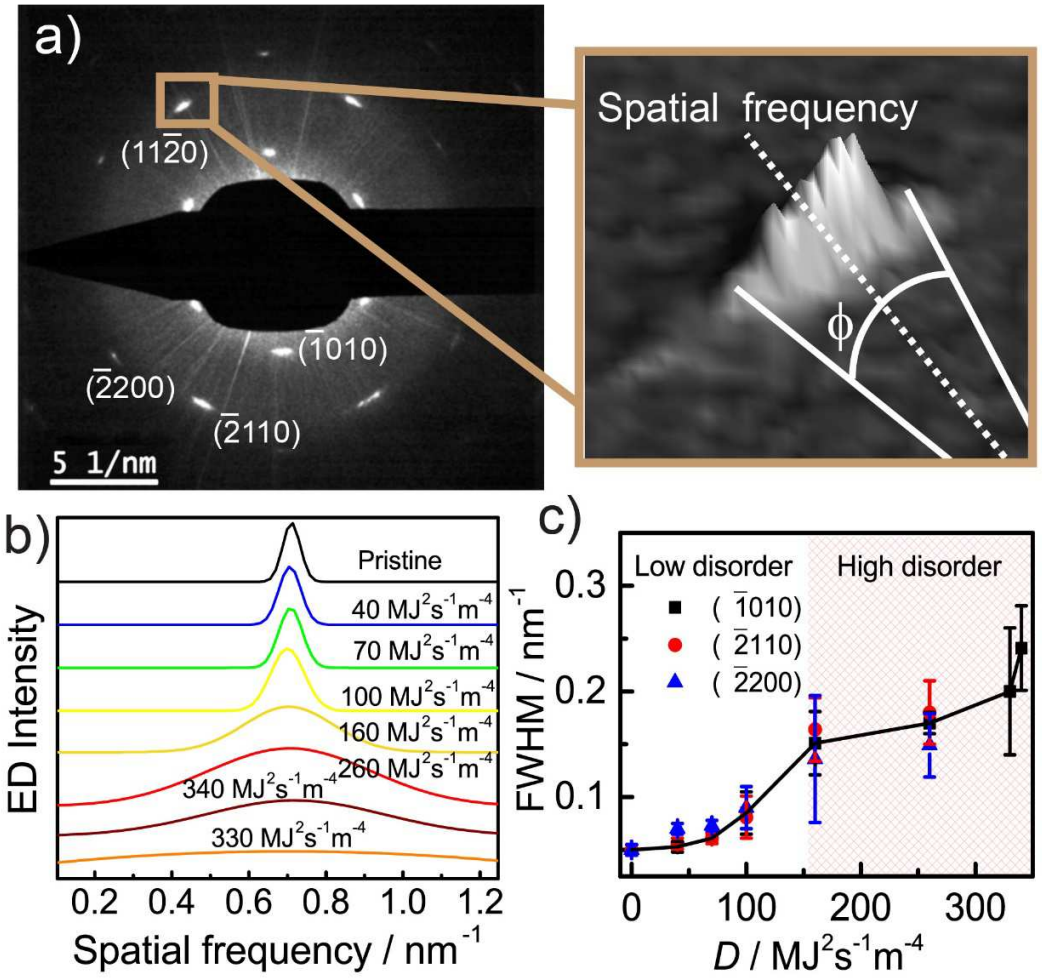

Fig 2. Electron diffraction features of two-photon oxidized graphene: a) The ED of the two-photon oxidized graphene at dose parameter *D* of 255 MJ^2/(s.m^4). Inset shows the 3-D intensity distribution of (11$\bar{2}$0) reflection, in which the electron counts are used as the third dimension. The radial direction (parallel to the reciprocal lattice vector) and streaking along the azimuthal direction (perpendicular to the reciprocal lattice vector) of the diffracted peaks are represented by dashed line and φ angle, respectively. b) The radial ED intensity profiles of the (11$\bar{2}$0) reflection for different irradiation doses. c) The respective FWHM values as a function of dose parameter *D*. Table S2 in the support information show the values used for this plot. The lines connecting the points are only guide for the eyes. The graphic is divided in two regimes, low disorder and high disorder, this point is further discussed in sections 3.3 and 3.4.

3.3 Chemical characterization

Oxygen functional groups in GO and reduced graphene oxide (RGO) are subjects debated in the literature [35-37] and the use of quantitative or semi-quantitative chemical analyses is still a topic of interest for these materials. In this work, to determine the chemical changes of irradiated graphene as function of irradiation dose, the core-loss regions of C, O and N EELS spectra were acquired and respective atomic contents were computed (the detailed quantitative analyses are summarized in Table S4 and the electron energy loss spectra are presented in Fig. S3 in the support information). Well-defined π^* and σ^* peaks in the region of C K-edge spectra were observed at low irradiation doses, while high irradiation doses produced a broadening of these peaks. The accuracy of theoretically calculated cross sections for quantitative chemical analysis using EELS for two dimensional materials such as graphene still needs to be improved. Therefore, we assumed that all computed cross sections contribute with blanket 10% uncertainty to the total error in the final quantitative results obtained by EELS analyses (see for instance Hartree-Slater model [38, 39]). This uncertainty is propagated through calculations that make use of computed cross sections [39-41]. See support information for more details.

The obtained relative amount of oxygen increases as a function of irradiation dose starting from the beginning of the irradiation by laser (see in Fig. 3). This result undoubtedly demonstrates that the oxidation of graphene is driven by two-photon absorption process. The amount of nitrogen remained at the same level near the detection limit of the method of the analysis for all irradiation doses. The presence of nitrogen in the sample can be attributed to its adsorption from atmosphere either upon synthesis or during the oxidation process. A comprehensive discussion about atoms adsorbed in graphene can be found elsewhere [42]. Another important observation is related to the oxygen obtained for pristine graphene. In order to separate the sample's effect, we collected EELS spectra from highly crystalline graphene regions of 10 nm × 10 nm and obtained the amount of oxygen in these regions of less than 2%. Consequently, the oxygen measured in pristine graphene most likely comes from polymer residues (typically PMMA) used to transfer graphene to the TEM grid. Therefore, we applied a correction to the O/C ratios taking into account the evaporation of PMMA with increasing

irradiation dose). See support information for the details of the correction procedure. Fig. 3 shows the corrected O/C ratio values. By considering that PMMA is covering 50 % (from Fig. 1g) of the pristine graphene with an O/C measured ratio of 27%, we estimate a PMMA average thickness of about 3 nm, which is a reasonable value for the contrast in the TEM images. Indeed, after transferring CVD graphene the polymer residues is one of the drawbacks for large area single layer graphene applications [43]. One can see that O/C ratio shows a trend to saturation at high irradiation doses. This behavior is, most probably, due to the decreasing amount of not oxidized carbon atoms available for two-photon absorption with increasing irradiation dose. The saturation effect becomes more pronounced for the dose parameters higher than 163 $MJ^2/(s.m^4)$. It is worth noting that this level of irradiation delimits the regime of irradiation characterized by initiation of pores growth, as observed in HRTEM studies, and by an active disordering of graphene structure, as indicated by FWHM values of ED measurements. Consequently, the laser irradiation of graphene to the dose parameters below 163 $MJ^2/(s.m^4)$ can be classified as a low dose regime (low disorder) and above 163 $MJ^2/(s.m^4)$ as a high dose regime (high disorder) of graphene irradiation.

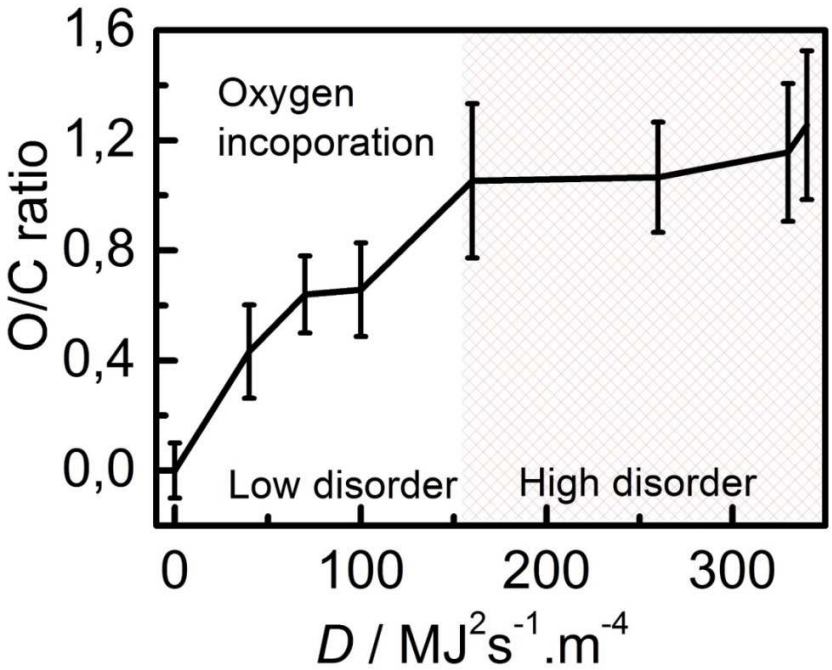

Fig. 3. EELS semi-quantitative analyses of the O/C (oxygen to carbon) atomic ratio of the two-photon oxidized graphene in function of laser dose parameter *D*. The O/C ratio increases up to one where it reaches the limit of the low and high disorder regimes.

3.4 Raman spectroscopy

The Raman spectrum of crystalline graphene is well known [44] showing two most prominent bands, namely the G band centered near 1580 cm^{-1} and the 2D band centered near 2700 cm^{-1}. The G band is a first order E_{2g} symmetry normal optical mode at the center of the Brillouin zone (BZ) originated by in-plane C-C stretching. The 2D band is a second order of the double-resonant D Raman mode [45] assigned to in-plane transverse optical phonons near the K point of the BZ [46]. The D band is only observable in the presence of disorder in the crystalline structure, where defects act as scattering centers for electrons involved in electron-phonon scattering. The D band appears at approximately 1350 cm^{-1} for an excitation laser of 2.33 eV (532 nm). In the presence of a disorder, a less intense band, called D', is also observed near 1620 cm^{-1}. Like the D band, D' is also a defect-induced double-resonant Raman mode. The intensity of the D band has long been used as a measure of disorder in carbon materials [47] and a simple mathematical relation between the ratio of the intensities of the D and G bands and the mean crystallite size, L_a, of polycrystalline graphite was found. This idea was further used [48] to study amorphous carbon, and was only valid for L_a greater than a few nanometers (2 nm ~ 3 nm). For amorphous carbon, whose L_a is typically smaller than 2 nm, a new mathematical relation was used [9, 10]. Recently, a phenomenological description for single defects [9] on a monolayer graphene established a deterministic relation of the I(D)/I(G) ratio with the mean distance between defects, L_D. In the same path, a more detailed description of the relation between the crystallite size of different heat-treated diamond-like carbon (DLC) samples and their Raman spectra was proposed [49]. Similar results were also found for oxidized graphene produced by plasma etching [50]. In all cases, one first observes a rise in I(D)/I(G) ratio correlated with the increasing disorder or oxidation level and, after some maximum value, the I(D)/I(G) ratio starts to decrease as the graphene structure evolve towards an amorphous state. When we have mixed types of defects, it is more appropriate to evaluate a disorder state of graphene from Raman data by plotting I(D)/I(G) ratio as a function of G band width [51]. In this plot, one can distinguish two different structural regimes of graphene representing low disorder and high disorder (see Fig. 4b). Moreover, from this plot one can judge about the character (one or zero-dimensional) of structural imperfections present in the graphene sample. The I(D')/I(G) ratio also shows a similar behavior in the equivalent plot. It is worth noting that D' band intensity also depends on the disorder level as well on the type of the defects [52]. For instance, for sp^3-type defects, such as in

oxidation, I(D)/I(D') is around 13; for vacancy-type (low dose ion bombardment), I(D)/I(D') is around 7; and for boundary defects, I(D)/I(D') is near 3.5.

Fig. 4a shows the typical Raman spectra of graphene irradiated to a specific dose together with the spectrum of the pristine graphene. The spectra were normalized by the G band intensity for the sake of comparison. One can see that the spectrum of pristine graphene already has a weak D band. This is typical of CVD grown graphene contamination by hydrocarbons, which occasionally form C-C bonds to graphene [4]. As the irradiation dose increases, the intensity of the D band increases accordingly and also does the width of both D and G bands, showing that the system is becoming more disordered. For a dose D = 255 $MJ^2/(s.m^4)$ and higher, the D band intensity starts do decrease, indicating that the system reached the maximum of the I(D)/I(G) curve, and the graphene is becoming amorphous.

Fig. 4b shows the plot of I(D)/I(G) versus G band width, Γ_G. Different square symbols with same color represent spectra acquired at different parts of the sample subjected to the same dose. A theoretically calculated dashed curve is superposed on experimentally obtained data points in the plot. This curve was adapted from Eq. (8) of Ref. [9], where L_D was replaced by $(\Gamma_G-\Gamma_0)^{-1}$, and Γ_0 =12 cm^{-1} is the G band width of pristine graphene. This is justifiable because it is well known that Γ_G always increases with the level of disorder, that means, it is inversely proportional to any disorder length, either L_D [10] or L_a [49]. This is a simple approximation, because in the present case the type of defects occurring predominantly for a given dose is changing, as it will be clear in the following paragraphs.

The experimental data points follow fairly well the theoretical curve up to dose parameter of 163 $MJ^2/(s.m^4)$. At this dose one observes a considerable scattering of the data depending on the probed region of the sample. We attribute this behavior to the formation of a considerable number of one-dimensional defects that form at this dose level and that may reduce substantially I(D)/I(G) ratio. Their spatial distribution is strongly heterogeneous at the scale of the size of the Raman laser beam. As a consequence, significantly different amounts of one-dimensional defects are probed from region to region causing data scattering in the plot.

The I(D)/I(D') ratio plotted as function of the dose parameter provides an additional insight into the evolution of defects during irradiation (see Fig. 4c). This ratio starts at expected "infinite" (around 70) value for pristine graphene and reduces down to 2 for the highest

irradiation dose of this study. A nearly linear reduction of I(D)/I(D') ratio with increasing irradiation dose follows up to dose parameter of 104 $MJ^2/(s.m^4)$. At this dose the I(D)/I(D') ratio was 13. Further increase of irradiation dose results in a much slower decrease of I(D)/I(D') ratio. At the dose parameter of 163 $MJ^2/(s.m^4)$ which delimits the low and high disorder in graphene structure, the I(D)/I(D') ratio was close to 7.

The above results are consistent with the previous study [53]. The initial stage of irradiation results in a formation of sp^3-type defects corresponding to the oxidation of graphene. After certain irradiation dose, other types of defects like vacancies and vacancy clusters are formed and dominate the defect structure of graphene. The further vacancy clusters growth and concomitant fragmentation of graphene domains results in predomination of boundary defects on the I(D)/I(D') ratio at highest irradiation doses of this study. This scenario of structural evolution is in a good agreement with the results of all measurements of this work.

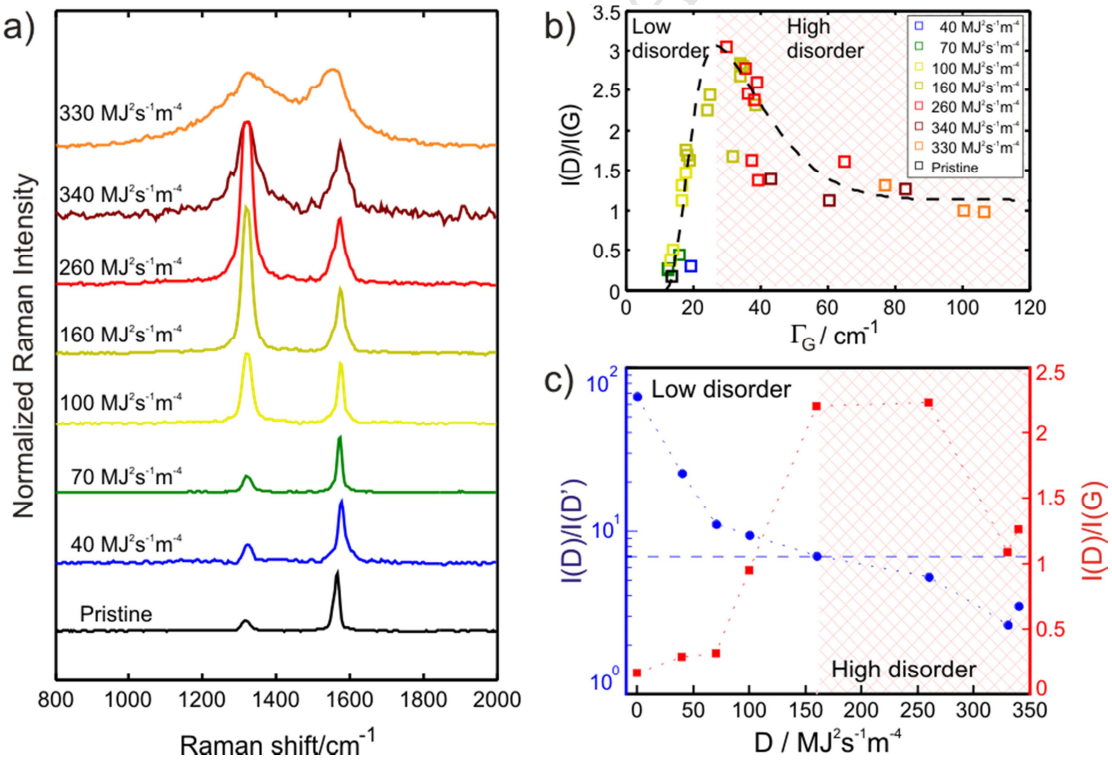

Fig. 4 – Raman spectroscopy analyses of two-photon oxidized graphene. (a) Typical Raman spectra of the different samples showing the main D and G bands. The D' band is typically very weak, so it can hardly be seen in this scale. (b) D and G band intensities ratio versus G band

width. Data obtained by fitting the Raman spectra with Lorentzian curves. The maximum of the curve separates the low and high disorder regimes. (c) Mean values of I(D)/I(D') (● symbol, left axis) and I(D)/I(G) (■ symbol, right axis) as a function of laser dose parameter *D*. The dashed blue line corresponds to I(D)/I(D') = 7, and this is a threshold between two different types of defects, which also correspond to the separation of the two disorder regimes.

4. Discussion on a structural implication of oxygen incorporation in graphene via two-photon oxidization.

Two-photon oxidation of graphene has already proven to be a reliable all optical method to create graphene devices at sub micrometer scale. The obtained results show that it can be also used as a reference method to model and to understand structural and morphological changes that occur during the oxygen incorporation in graphene. To our knowledge, conventional chemical methods cannot produce GO with oxidation level varying as much as the two-photon oxidation method does. The obtained results show that the oxidation of graphene induced by laser irradiation can be divided into three regimes according to the produced irradiation effects: 1) nearly constant oxidation rate as a function of irradiation dose (low irradiation dose regime at dose parameters *D* below 104 $MJ^2/(s.m^4)$); 2) saturation stage of sp^3-type defects formation accompanied by point defects formation and nucleation of pores (intermediate irradiation dose regime at 104 $MJ^2/(s.m^4) < D < 255$ $MJ^2/(s.m^4)$); and 3) boundary defects formation as a result of pores growth and fragmentation of graphene domains (high irradiation dose regime at *D* above 255 $MJ^2/(s.m^4)$).

During the first regime, one identifies highly ordered crystalline domains of the graphene structure via HRTEM, the ED patterns cannot be clearly distinguished from the one of pristine graphene and the O/C atomic ratio stays bellow 0.5. Through Raman spectroscopy one sees a low disorder regime and the defects are identified as of sp^3-type indicating the formation of oxygen functional groups in the graphene structure. This regime of irradiation modifies graphene in a way similar to conventional chemical methods of GO production.

During the intermediate regime, the crystalline regions become scarce in HRTEM, pores with diameter of up to about 10 nm are present in the sample, the ED spots exhibit a clear broadening, and the oxygen to carbon ratio becomes higher than 0.5. With Raman spectroscopy,

one identifies a transition from low to high structural disorder driven by the formation of vacancy type defects in graphene lattice. At this regime the two-photon oxidation of graphene samples starts to make profound modifications in their structure, and the level of oxidation is undoubtedly higher than those achieved via conventional chemical methods. The origin of pores might result from structural instabilities (breakage) of C-C bonds of aromatic carbon rings due to formation of reactive oxygen species such as hydroxyl radicals. At early stages of oxidation, epoxide and hydroxyl groups are formed in the basal plane of graphene. When all sites of basal plane are functionalized with these groups, the excess oxidant attacks them, and may produce high energy peroxide bridges C-O-O-C which are a well-known source of reactive oxygen species such as hydroxyl radicals [54]. Indeed, in a previous work [17], it was found that for graphene supported on Si/SiO2, oxidation propagates in an island-like fashion, i.e. oxidation initially happens randomly but then islands get heavily oxidized while the region between them remains less oxidized. Eventually, formed nitrogen bridges and other nitrogen functionalities may also act as catalyst to reduce the energy barrier for C-C bonds rearrangement or breakage [55].

During the third irradiation regime, the structure of oxidized graphene sample exhibits amorphous and crystalline phases, the sheet morphology is replete of pores from a few nanometers up to 100 nm and higher, the graphene ED spots continue to broaden. Diffraction spots radial streaking tends to form powder diffraction rings as a consequence of graphene domains fragmentation, their rotating and buckling. At this regime, the amount of incorporated oxygen stays nearly fixed, having an oxygen to carbon ratio close to one, which is probably the highest concentration of oxygen supported by graphene before carbon evaporation. Via Raman spectroscopy one identifies a high disorder regime where boundary defects dominate the overall defect structure of graphene.

5. Conclusions

In this work we studied the structural and chemical changes of graphene oxidized by means of the laser induced two-photon absorption process using HRTEM, ED, EELS and Raman spectroscopy. The oxygen incorporation in graphene increases at nearly constant rate until it reaches an O/C atomic ratio of about one. This happens in the low and intermediate irradiation

dose of graphene, which we identified as a low disorder regime. At higher irradiation doses the structure of the oxidized graphene sample undergoes a profound modification moving from a low disorder regime to a high disorder regime characterized by the formation of an amorphous structure, with pores and domain fragmentation, accompanied by rotation and buckling. The low disorder state of graphene during the initial stage of the two-photon process is similar to a conventional chemical oxidation of graphene. This irradiation regime results in a creation of sp^3-type of defects, whereas during the high irradiation dose vacancies and boundaries become the main type of defects in graphene subsystem. We believe that the obtained results contribute to a harmonization in definitions of the oxidation states of graphene and to a formation of a unified basis for comparison of results on studies of GO, where different levels of oxidation might bring desired chemical, biological, structural and morphological functionalities.

References

[1] A.K. Geim, I.V. Grigorieva, Van der Waals heterostructures, Nature 499(7459) (2013) 419-425.
[2] A.K. Geim, K.S. Novoselov, The rise of graphene, Nat. Mater. 6(3) (2007) 183-191.
[3] F. Bonaccorso, L. Colombo, G.H. Yu, M. Stoller, V. Tozzini, A.C. Ferrari, R.S. Ruoff, V. Pellegrini, Graphene, related two-dimensional crystals, and hybrid systems for energy conversion and storage, Science 347(6217) (2015).
[4] R.K. de Castro, J.R. Araujo, R. Valaski, L.O.O. Costa, B.S. Archanjo, B. Fragneaud, M. Cremona, C.A. Achete, New transfer method of CVD-grown graphene using a flexible, transparent and conductive polyaniline-rubber thin film for organic electronic applications, Chem. Eng. J. 273 (2015) 509-518.
[5] M. Terrones, A.R. Botello-Mendez, J. Campos-Delgado, F. Lopez-Urias, Y.I. Vega-Cantu, F.J. Rodriguez-Macias, A.L. Elias, E. Munoz-Sandoval, A.G. Cano-Marquez, J.C. Charlier, H. Terrones, Graphene and graphite nanoribbons: Morphology, properties, synthesis, defects and applications, Nano Today 5(4) (2010) 351-372.
[6] B.S. Archanjo, A.P.M. Barboza, B.R.A. Neves, L.M. Malard, E.H.M. Ferreira, J.C. Brant, E.S. Alves, F. Plentz, V. Carozo, B. Fragneaud, I.O. Maciel, C.M. Almeida, A. Jorio, C.A. Achete, The use of a Ga+ focused ion beam to modify graphene for device applications, Nanotechnology 23(25) (2012).
[7] B.S. Archanjo, B. Fragneaud, L.G. Cancado, D. Winston, F. Miao, C.A. Achete, G. Medeiros-Ribeiro, Graphene nanoribbon superlattices fabricated via He ion lithography, Appl. Phys. Lett. 104(19) (2014).
[8] A. Johansson, P. Myllyperkiö, P. Koskinen, J. Aumanen, J. Koivistoinen, H.-C. Tsai, C.-H. Chen, L.-Y. Chang, V.-M. Hiltunen, J.J. Manninen, W.Y. Woon, M. Pettersson, Optical Forging of Graphene into Three-Dimensional Shapes, Nano Lett. 17(10) (2017) 6469-6474.
[9] M.M. Lucchese, F. Stavale, E.H.M. Ferreira, C. Vilani, M.V.O. Moutinho, R.B. Capaz, C.A. Achete, A. Jorio, Quantifying ion-induced defects and Raman relaxation length in graphene, Carbon 48(5) (2010) 1592-1597.
[10] E.H. Martins Ferreira, M.V.O. Moutinho, F. Stavale, M.M. Lucchese, R.B. Capaz, C.A. Achete, A. Jorio, Evolution of the Raman spectra from single-, few-, and many-layer graphene with increasing disorder, Phys. Rev. B 82(12) (2010) 125429.

[11] F. Banhart, J. Kotakoski, A.V. Krasheninnikov, Structural Defects in Graphene, Acs Nano 5(1) (2011) 26-41.
[12] A. Narita, X.Y. Wang, X.L. Feng, K. Mullen, New advances in nanographene chemistry, Chem. Soc. Rev. 44(18) (2015) 6616-6643.
[13] Q. Tang, Z. Zhou, Z.F. Chen, Graphene-related nanomaterials: tuning properties by functionalization, Nanoscale 5(11) (2013) 4541-4583.
[14] K.L.S. Castro, R.V. Curti, J.R. Araujo, S.M. Landi, E.H.M. Ferreira, R.S. Neves, A. Kuznetsov, L.A. Sena, B.S. Archanjo, C.A. Achete, Calcium incorporation in graphene oxide particles: A morphological, chemical, electrical, and thermal study, Thin Solid Films 610 (2016) 10-18.
[15] D.R. Dreyer, S. Park, C.W. Bielawski, R.S. Ruoff, The chemistry of graphene oxide, Chem. Soc. Rev. 39(1) (2010) 228-240.
[16] J. Aumanen, A. Johansson, J. Koivistoinen, P. Myllyperkio, M. Pettersson, Patterning and tuning of electrical and optical properties of graphene by laser induced two-photon oxidation, Nanoscale 7(7) (2015) 2851-2855.
[17] J. Koivistoinen, L. Sladkova, J. Aumanen, P. Koskinen, K. Roberts, A. Johansson, P. Myllyperkio, M. Pettersson, From Seeds to Islands: Growth of Oxidized Graphene by Two-Photon Oxidation, J. Phys. Chem. B 120(39) (2016) 22330-22341.
[18] A. Johansson, H.-C. Tsai, J. Aumanen, J. Koivistoinen, P. Myllyperkiö, Y.-Z. Hung, M.-C. Chuang, C.-H. Chen, W.Y. Woon, M. Pettersson, Chemical composition of two-photon oxidized graphene, Carbon 115 (2017) 77-82.
[19] J. Koivistoinen, P. Myllyperkio, M. Pettersson, Time-Resolved Coherent Anti-Stokes Raman Scattering of Graphene: Dephasing Dynamics of Optical Phonon, Journal of Physical Chemistry Letters 8(17) (2017) 4108-4112.
[20] H.J. Park, J. Meyer, S. Roth, V. Skakalova, Growth and properties of few-layer graphene prepared by chemical vapor deposition, Carbon 48(4) (2010) 1088-1094.
[21] V. Swamy, A. Kuznetsov, L.S. Dubrovinsky, P.F. McMillan, V.B. Prakapenka, G. Shen, B.C. Muddle, Size-dependent pressure-induced amorphization in nanoscale TiO2, Phys. Rev. Lett. 96(13) (2006).
[22] G.K. Williamson, W.H. Hall, X-ray line broadening from filed aluminium and wolfram, Acta Metall. 1(1) (1953) 22-31.
[23] A.S. Avilov, S.P. Gubin, M.A. Zaporozhets, Electron crystallography as an informative method for studying the structure of nanoparticles, Crystallogr. Rep. 58(6) (2013) 788-804.
[24] T.E. Weirich, M. Winterer, S. Seifried, H. Hahn, H. Fuess, Rietveld analysis of electron powder diffraction data from nanocrystalline anatase, TiO2, Ultramicroscopy 81(3) (2000) 263-270.
[25] C. Gammer, C. Mangler, C. Rentenberger, H.P. Karnthaler, Quantitative local profile analysis of nanomaterials by electron diffraction, Scripta Mater. 63(3) (2010) 312-315.
[26] B.E. Warren, X-ray Diffraction, Addison-Wesley, New york, 1969.
[27] S.-C. Tsai, E.W. Huang, J.-J. Kai, F.-R. Chen, Microstructural evolution of nuclear grade graphite induced by ion irradiation at high temperature environment, J. Nucl. Mater. 434(1–3) (2013) 17-23.
[28] J.C. Meyer, A.K. Geim, M.I. Katsnelson, K.S. Novoselov, D. Obergfell, S. Roth, C. Girit, A. Zettl, On the roughness of single- and bi-layer graphene membranes, Solid State Commun. 143(1-2) (2007) 101-109.
[29] C.T. Pan, J.A. Hinks, Q.M. Ramasse, G. Greaves, U. Bangert, S.E. Donnelly, S.J. Haigh, In-situ observation and atomic resolution imaging of the ion irradiation induced amorphisation of graphene, Sci. Rep. 4 (2014) 6334.
[30] N.R. Wilson, P.A. Pandey, R. Beanland, J.P. Rourke, U. Lupo, G. Rowlands, R.A. Romer, On the structure and topography of free-standing chemically modified graphene, New J. Phys. 12 (2010).
[31] N.R. Wilson, P.A. Pandey, R. Beanland, R.J. Young, I.A. Kinloch, L. Gong, Z. Liu, K. Suenaga, J.P. Rourke, S.J. York, J. Sloan, Graphene Oxide: Structural Analysis and Application as a Highly Transparent Support for Electron Microscopy, Acs Nano 3(9) (2009) 2547-2556.

[32] K. Erickson, R. Erni, Z. Lee, N. Alem, W. Gannett, A. Zettl, Determination of the Local Chemical Structure of Graphene Oxide and Reduced Graphene Oxide, Adv. Mater. 22(40) (2010) 4467-4472.
[33] C. Gomez-Navarro, J.C. Meyer, R.S. Sundaram, A. Chuvilin, S. Kurasch, M. Burghard, K. Kern, U. Kaiser, Atomic Structure of Reduced Graphene Oxide, Nano Lett. 10(4) (2010) 1144-1148.
[34] D.B. Williams, C.B. Carter, Transmission Electron Microscopy: A Textbook for Materials Science, Springer US2013.
[35] D. Pacilé, J.C. Meyer, A. Fraile Rodríguez, M. Papagno, C. Gómez-Navarro, R.S. Sundaram, M. Burghard, K. Kern, C. Carbone, U. Kaiser, Electronic properties and atomic structure of graphene oxide membranes, Carbon 49(3) (2011) 966-972.
[36] A. Tararan, A. Zobelli, A.M. Benito, W.K. Maser, O. Stéphan, Revisiting Graphene Oxide Chemistry via Spatially-Resolved Electron Energy Loss Spectroscopy, Chem. Mater. 28(11) (2016) 3741-3748.
[37] N. Morimoto, T. Kubo, Y. Nishina, Tailoring the Oxygen Content of Graphite and Reduced Graphene Oxide for Specific Applications, Sci. Rep. 6 (2016) 21715.
[38] H. Kohl, A SIMPLE PROCEDURE FOR EVALUATING EFFECTIVE SCATTERING CROSS-SECTIONS IN STEM, Ultramicroscopy 16(2) (1985) 265-268.
[39] C.C. Ahn, P. Rez, Inner shell edge profiles in electron energy loss spectroscopy, Ultramicroscopy 17(2) (1985) 105-115.
[40] R. Brydson, Electron Energy Loss Spectroscopy, BIOS Scientific Publishers2001.
[41] R.D. Leapman, P. Rez, D.F. Mayers, K, L, and M shell generalized oscillator strengths and ionization cross sections for fast electron collisions, J. Chem. Phys. 72(2) (1980) 1232-1243.
[42] I.A. Pašti, A. Jovanović, A.S. Dobrota, S.V. Mentus, B. Johansson, N.V. Skorodumova, Atomic adsorption on pristine graphene along the Periodic Table of Elements – From PBE to non-local functionals, Appl. Surf. Sci. 436 (2018) 433-440.
[43] J. Kang, D. Shin, S. Bae, B.H. Hong, Graphene transfer: key for applications, Nanoscale 4(18) (2012) 5527-5537.
[44] A.C. Ferrari, J.C. Meyer, V. Scardaci, C. Casiraghi, M. Lazzeri, F. Mauri, S. Piscanec, D. Jiang, K.S. Novoselov, S. Roth, A.K. Geim, Raman Spectrum of Graphene and Graphene Layers, Phys. Rev. Lett. 97(18) (2006) 187401.
[45] C. Thomsen, S. Reich, Double Resonant Raman Scattering in Graphite, Phys. Rev. Lett. 85(24) (2000) 5214-5217.
[46] R. Saito, A. Jorio, A.G. Souza Filho, G. Dresselhaus, M.S. Dresselhaus, M.A. Pimenta, Probing Phonon Dispersion Relations of Graphite by Double Resonance Raman Scattering, Phys. Rev. Lett. 88(2) (2001) 027401.
[47] F. Tuinstra, J.L. Koenig, Raman Spectrum of Graphite, J. Chem. Phys. 53(3) (1970) 1126-1130.
[48] A.C. Ferrari, J. Robertson, Interpretation of Raman spectra of disordered and amorphous carbon, Phys. Rev. B 61(20) (2000) 14095-14107.
[49] J. Ribeiro-Soares, M.E. Oliveros, C. Garin, M.V. David, L.G.P. Martins, C.A. Almeida, E.H. Martins-Ferreira, K. Takai, T. Enoki, R. Magalhães-Paniago, A. Malachias, A. Jorio, B.S. Archanjo, C.A. Achete, L.G. Cançado, Structural analysis of polycrystalline graphene systems by Raman spectroscopy, Carbon 95 (2015) 646-652.
[50] I. Childres, L.A. Jauregui, J. Tian, Y.P. Chen, Effect of oxygen plasma etching on graphene studied using Raman spectroscopy and electronic transport measurements, New J. Phys. 13 (2011).
[51] C. Luiz Gustavo, S. Mateus Gomes da, H.M.F. Erlon, H. Ferdinand, K. Katerina, H. Kai, P. Alain, A. Carlos Alberto, B.C. Rodrigo, J. Ado, Disentangling contributions of point and line defects in the Raman spectra of graphene-related materials, 2D Materials 4(2) (2017) 025039.
[52] A. Eckmann, A. Felten, A. Mishchenko, L. Britnell, R. Krupke, K.S. Novoselov, C. Casiraghi, Probing the Nature of Defects in Graphene by Raman Spectroscopy, Nano Lett. 12(8) (2012) 3925-3930.

[53] A. Zandiatashbar, G.H. Lee, S.J. An, S. Lee, N. Mathew, M. Terrones, T. Hayashi, C.R. Picu, J. Hone, N. Koratkar, Effect of defects on the intrinsic strength and stiffness of graphene, Nat. Commun. 5 (2014).
[54] H.-K. Jeong, Y.P. Lee, R.J.W.E. Lahaye, M.-H. Park, K.H. An, I.J. Kim, C.-W. Yang, C.Y. Park, R.S. Ruoff, Y.H. Lee, Evidence of Graphitic AB Stacking Order of Graphite Oxides, J. Am. Chem. Soc. 130(4) (2008) 1362-1366.
[55] X.-F. Li, K.-Y. Lian, L. Liu, Y. Wu, Q. Qiu, J. Jiang, M. Deng, Y. Luo, Unraveling the formation mechanism of graphitic nitrogen-doping in thermally treated graphene with ammonia, Sci. Rep. 6 (2016) 23495.